Fortschritte der Physik

www.fp-journal.org

Progress of Physics

WILEY-VCH

Fortschr. Phys. **57**, No. 11 – 12, 1121 – 1132 (2009) / **DOI** 10.1002/prop.200900094

Optimizing atom interferometry on atom chips

Ulrich Hohenester[1,*], **Julian Grond**[1], and **Jörg Schmiedmayer**[2]

[1] Institut für Physik, Karl-Franzens-Universität Graz, Universitätsplatz 5, 8010 Graz, Austria
[2] Atominstitut der Österreichischen Universitäten, TU-Wien, Stadionallee 2, 1020 Wien, Austria

Received 18 April 2009, accepted 9 May 2009
Published online 13 October 2009

Key words BEC, atom chip, atom number squeezing, numerical optimization.
PACS 03.75.-b,39.20.+q,39.25.+k,02.60.Pn

We theoretically investigate the performance of atom interferometers based on ultracold atoms and atom chips. Within the framework of the Gross-Pitaevskii equation, we simulate the splitting and trapping of a condensate. Within the two-mode model and the multi-configurational Hartree method for Bosons, we investigate number squeezing and its impact on the interferometer performance. We show that optimized control strategies allow for efficient condensate trapping and number squeezing on short time scales.

1 Introduction

Interferometry with matter waves [1] is a very versatile tool with applications ranging from precision experiments to fundamental studies. Of special interest are interference experiments with degenerate many body quantum systems, where the interference itself reveals details of the quantum state and its dynamics [2, 3]. Atom chips [4–6] have proven to be a versatile tool for precise manipulation and interference experiments with ultracold atoms [7–9]. A key ingredient in these experiments is the beam splitter for trapped or guided atoms [10–12] and its characteristics. Number fluctuations induced by the splitting cause phase diffusion [13], which currently limits the coherence in trapped atom interferometers more than decoherence coming from magnetic noise from the close by surface [14]. In this paper we discuss different approaches to optimally split a quantum degenerate cloud of atoms, and ways how even coherence and number squeezing [13, 15, 16] can be controlled by applying optimal control techniques.

We have organized our paper as follows. In Sect. 2 we introduce the theoretical framework for the description of Bose Einstein condensates. Our description schemes comprise the Gross-Pitaevskii equation, which accounts for the mean-field dynamics of the condensate, the two-mode model, which accounts for the atom number dynamics close to the splitting point, and we finally combine the condensate and atom number dynamics within the multi configurational time dependent Hartree method for Bosons (MCTDHB). The latter approach allows us to simulate atom interferometry in atom chips in a realistic manner. In Sect. 3 we present results for condensate splitting. We show that too fast splitting leads to condensate oscillations in the split trap. These oscillations can be completely suppressed if we use more refined splitting protocols, which we derive within the framework of optimal control theory. Within the framework of the two mode model, we investigate the impact of atom number fluctuations on phase diffusion and explore quantum control techniques for achieving high number squeezing at short times. Finally, we use MCTDHB for a realistic modelling of condensate splitting for atom interferometry, and determine the resulting coherence factors. In Sect. 4 we summarize our results and draw some conclusions. Some details of our optimization approach are given in the appendix.

* Corresponding author E-mail: ulrich.hohenester@uni-graz.at, Phone: +43 316 380 5227, Fax: +43 316 380 9820

2 Theory

2.1 Model Hamiltonian

Our starting point is given by the many-body Hamiltonian in second-quantized form [17, 18]

$$\hat{H} = \int \hat{\Psi}^\dagger(x) \left[-\frac{1}{2}\nabla^2 + V_\lambda(x) \right] \hat{\Psi}(x)\, dx + \frac{U_0}{2} \int \hat{\Psi}^\dagger(x)\hat{\Psi}^\dagger(x)\hat{\Psi}(x)\hat{\Psi}(x)\, dx\,. \tag{1}$$

The first term on the rhs accounts for the kinetic energy and the magnetic confinement potential $V_\lambda(x)$. The control parameter $\lambda(t)$ describes the variation of the confining potential when changing the external parameters [5, 12] (for details see below). Through $\lambda(t)$ it is possible to manipulate the trapped Bose-Einstein condensate, e.g. to split it by varying the potential from a single to a double well. The second term on the rhs accounts for the atom-atom interactions, where we have chosen a contact potential approximation for the interatomic potential. The field operators $\hat{\Psi}(x)$ and $\hat{\Psi}^\dagger(x)$ obey the usual equal-time commutation relations. For convenience, we only consider a quasi-one-dimensional condensate along a single spatial direction x, and use units where $\hbar = 1$ and the mass of the atoms is set to one [19]. Our restriction to a single spatial dimension is justified for elongated condensates where the dynamics in the weakly confined longitudinal direction is much slower than in the splitting direction, as discussed in some detail in [20].

Different physical regimes emerge from Eq. (1) by restricting the field operators to a certain class of basis functions. First, the *Gross-Pitaevskii equation* [17] is obtained by assuming that all atoms reside in a single "orbital" $\psi(x,t)$. Correspondingly, the field operator is

$$\hat{\Psi}(x) = \hat{a}_0\, \psi(x,t)\,, \tag{2}$$

where $\hat{a}_0$ is the operator associated with the condensate. The Gross-Pitaevskii equation properly accounts for the mean-field dynamics of the condensate, described by the orbital $\psi(x,t)$, but cannot cope with correlation effects and fragmentation, where more than a single orbital becomes populated.

When splitting a condensate, the confinement potential is transformed from a single to a double well, and at some point the condensate breaks up into two parts, $\psi_L(x)$ and $\psi_R(x)$, which are localized in either the left or right well. In a mean-field approach, the wavefunction is a coherent superposition $\psi_L(x)+\psi_R(x)$ where all atoms are delocalized over the wells. The corresponding atom number distribution is a binomial one, since each atom has a fifty percent probability of localization in either the left or right well, and the fluctuations correspond to shot noise. On the other hand, the nonlinear interaction in Eq. (1) favors narrow atom number distributions, in order to minimize the atom-atom repulsion. Close to the splitting point, we can approximately ignore the dynamics of the orbitals $\psi_{L,R}(x)$, and recover the *two-mode approximation* [13, 21]

$$\hat{\Psi}(x) = \hat{a}_L\, \psi_L(x) + \hat{a}_R\, \psi_R(x)\,. \tag{3}$$

Here, the whole condensate dynamics is associated with the atom number distribution, through the field operators $\hat{a}_L$ and $\hat{a}_R$, whereas the orbital degrees of freedom are lumped into a few effective parameters (see Sect. 2.3 for details).

In the most general case, we can neither neglect the orbital nor the atom number dynamics. This can be done by choosing a field operator of the form

$$\hat{\Psi}(x) = \hat{a}_L(t)\, \psi_L(x,t) + \hat{a}_R(t)\, \psi_R(x,t)\,, \tag{4}$$

where $\psi_{L,R}(x,t)$ are time-dependent orbitals that have to be determined self-consistently. A convenient approach is provided by the *multi-configurational time dependent Hartree method for bosons (MCTDHB)* [22], which determines the orbitals from a variational principle. Quite generally, we could include more orbitals in Eq. (4), but we will stick to only $\psi_{L,R}(x,t)$ for reasons detailed below.

2.2 Gross-Pitaevskii equation

Let us first look more closely to the dynamic equations that emerge from the different field operators. In the case of the Gross-Pitaevskii equation, the number of atoms results in a mere multiplication factor of the nonlinear term in Eq. (1). More specifically, one gets after some straightforward manipulations the celebrated Gross-Pitaevskii equation [17, 18]

$$i\frac{\partial\psi(x,t)}{\partial t} = \left[-\frac{1}{2}\nabla^2 + V_\lambda(x) + U_0(N-1)\left|\psi(x,t)\right|^2\right]\psi(x,t)\,. \tag{5}$$

for the condensate wavefunction $\psi(x,t)$. The non-linear term on the rhs accounts in a mean-field manner for the repulsive atom interactions. From Eq. (5) we can also obtain an equation that describes the motion of condensate excitations, the so-called Bogoliubov-de Gennes equation, by considering a slightly perturbed wavefunction $\psi + \delta\psi$ and linearizing Eq. (5) with respect to $\delta\psi$ [18].

2.3 Two-mode approximation

In the two-mode model, we do not consider the dynamics of the orbitals but only the distribution of atoms between left and right well. The model is appropriate for the description of condensate splitting close to the splitting point. Its framework is reminiscent of the Josephson physics, where Cooper pairs can tunnel back and forth between two weakly coupled superconductors. Let us investigate the basic Hamiltonian first. Upon insertion of the field operator (3) into the many-body Hamiltonian of Eq. (1), we get [21]

$$\hat{H} = -\frac{\Omega}{2}\left(\hat{a}_L^\dagger\hat{a}_R + \hat{a}_R^\dagger\hat{a}_L\right) + \kappa\left(\hat{a}_L^\dagger\hat{a}_L^\dagger\hat{a}_L\hat{a}_L + \hat{a}_R^\dagger\hat{a}_R^\dagger\hat{a}_R\hat{a}_R\right)\,. \tag{6}$$

Here, the first term on the rhs accounts for tunneling between the two wells, with the tunnel matrix element $\Omega = \langle\psi_L|\left(-\nabla^2/2 + V_\lambda\right)|\psi_R\rangle$ + c.c., and the second term for the nonlinear coupling, with $\kappa = (U_0/2)\int\left|\psi_{L,R}(x)\right|^4 dx$ being the nonlinearity parameter. In Eq. (6) we have neglected all inter-well couplings and contributions proportional to the total atom number operator, which do not contribute to the dynamics.

Within the two mode model, one usually assumes that the tunnel coupling Ω can be modified by slightly varying the double-well potential V_λ, through the control parameter $\lambda(t)$. In contrast, the nonlinearity κ is assumed to be not affected by such variations. This is a reasonable assumption since Ω accounts for a tunneling process, whose efficiency depends extremely sensitive on the details of the potential, whereas κ is expected to be rather insensitive to slight modifications of V_λ. In the following we consider $\Omega(t)$ as a time-dependent control parameter. We also set $2\kappa N = 1$, where N is the total number of atoms in the trap, which corresponds to a mere rescaling of the energy and time scales.

The atom number distribution can be expanded in a basis

$$|m\rangle = \left[\left(\frac{N}{2}+m\right)!\left(\frac{N}{2}-m\right)!\right]^{-\frac{1}{2}}\left(\hat{a}_L^\dagger\right)^{\frac{N}{2}+m}\left(\hat{a}_R^\dagger\right)^{\frac{N}{2}-m}|0\rangle\,. \tag{7}$$

Here m is the *atom number imbalance* between the left and right well, with $(N/2)+m$ atoms in the left and $(N/2)-m$ atoms in the right well, which takes for an even number of atoms values between $-(N/2)$ and $(N/2)$. The total wavefunction is of the form $|C\rangle = \sum_m C_m(t)\,|m\rangle$. Its equation of motion is given by the Schrödinger equation with the two-mode Hamiltonian of Eq. (6).

The two mode model can be mapped onto an angular-momentum pseudospin model, with the total angular momentum $N/2$ and the projection on the z-axis corresponding to the atom number imbalance m. The angular momentum operators are then expressed in the Schwinger boson representation viz.

$$\hat{J}_x = \frac{1}{2}\left(\hat{a}_L^\dagger\hat{a}_R + \hat{a}_R^\dagger\hat{a}_L\right)\,,\quad \hat{J}_y = -\frac{i}{2}\left(\hat{a}_L^\dagger\hat{a}_R - \hat{a}_R^\dagger\hat{a}_L\right)\,,\quad \hat{J}_z = \frac{1}{2}\left(\hat{a}_L^\dagger\hat{a}_L - \hat{a}_R^\dagger\hat{a}_R\right)\,. \tag{8}$$

$\hat{J}_x$ promotes an atom from the left to the right well, or vice versa, and $\hat{J}_z$ measures the atom number difference between the two wells. By construction, the pseudospin operators fulfill the SU(2) commutation relations $[\hat{J}_i, \hat{J}_j] = i\epsilon_{ijk}\hat{J}_k$ with the totally antisymmetric Levi-Cevita tensor ϵ_{ijk}. Along the same lines, one can map the atom-number wavefunction C onto the unit sphere [23]. This will prove useful for the purpose of visualization. Within the pseudospin framework, the two-mode Hamiltonian becomes

$$\hat{H} = -\Omega(t)\hat{J}_x + 2\kappa\hat{J}_z^2\,. \tag{9}$$

This form of the Hamiltonian is completely analogous to the Josephson Hamiltonian, where $\Omega(t)$ is associated with the (time-dependent) Josephson energy and the nonlinearity κ with the charging energy.

2.4 Multi-configurational Hartree method for Bosons (MCTDHB)

We finally extend the two-mode model to the case where the two orbitals $\psi_L(x,t)$ and $\psi_R(x,t)$ can vary in time. In this case, we additionally need a prescription of how to determine the orbitals in "the best way". A convenient approach is provided by the multi-configurational time dependent Hartree method for bosons (MCTDHB) [22]. For the sake of shortness, in the following we only sketch the basic ideas and refer the interested reader for further details to the literature [22]. MCTDHB is based on a variational principle where the wavefunction is expanded in a certain basis of orbitals, in the most simple case two. Two orbitals are sufficient for the description of condensate splitting, but cannot account for fragmentation within the respective wells. Similar to the two-mode model, we can expand the atom-number part of the total wavefunction C in terms of m. The total wavefunction Ψ is then composed of C and the two time-dependent orbitals $\psi_{L,R}(x,t)$. The time evolutions of C and $\psi_{L,R}(x)$ are obtained from a Lagrange function by utilizing the Dirac-Frenkel variational principle [20, 22]. For the atom number part, we obtain a Schrödinger equation with a Hamiltonian similar to the two-mode model, Eq. (9). For the orbitals we obtain two non-linear Schrödinger-like equations, which are mutually coupled through the atom-atom interaction.

3 Results for condensate splitting

In our simulations we consider a confinement potential $V_\lambda(x)$ which can be deformed from a single well to a double well, by variation of λ. Fig. 1 shows $V_\lambda(x)$ for selected values of λ, and provides further details in the caption.

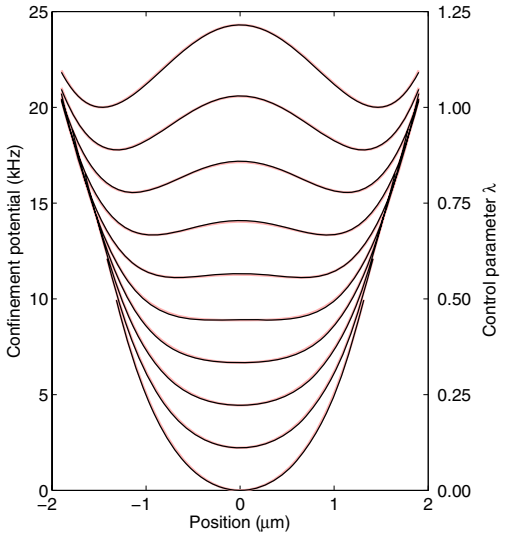

Fig. 1 In our simulations we consider ^{87}Rb atoms and the radio-frequency double-well confinement of Lesanovsky *et al.* [12], which is produced by a surface-mounted wire structure on an atom chip. We use the same parameters as given in [12], and vary the rf field strength by means of the control parameter λ according to $B_{\rm rf} = 0.5 + \lambda \times 0.3$ G. The figure shows the transformation of the confinement potential from a single to a double well. The different potential curves are offset for clarity. The offset corresponds to the value of the control parameter $\lambda(t)$. We also show a fit of $V_\lambda(x)$ to a generic confinement potential of the form $ax^2 + bx^4$ (bright lines, almost indistinguishable).

3.1 Gross-Pitaevskii description

Let us first consider condensate splitting within the framework of the Gross-Pitaevskii equation. Fig. 2(a) shows results of a simulation where the control parameter is varied according $\lambda \propto \sqrt{t}$ from zero to one, such that the potential is deformed within 2 ms from a single to a double well. The middle panel of the figure depicts a density plot of the wavefunction. One observes that the wavefunction is initially localized in the single well, and at later times splits into a left and right part. However, because the splitting is rather fast, the condensate ends up in an excited state of the split potential and continues to oscillate in the wells.

This is seen even more clearly in the Wigner function plots on the lhs of the figure. The Wigner function

$$W(x,p,t) = \int e^{-ips}\psi(x+\frac{s}{2},t)\psi^*(x-\frac{s}{2},t)\,ds \tag{10}$$

is a mixed position-momentum distribution, which has many appealing features. First, the Wigner function directly displays the motional state of the condensate. For instance, at $t = 1$ ms the Wigner function for

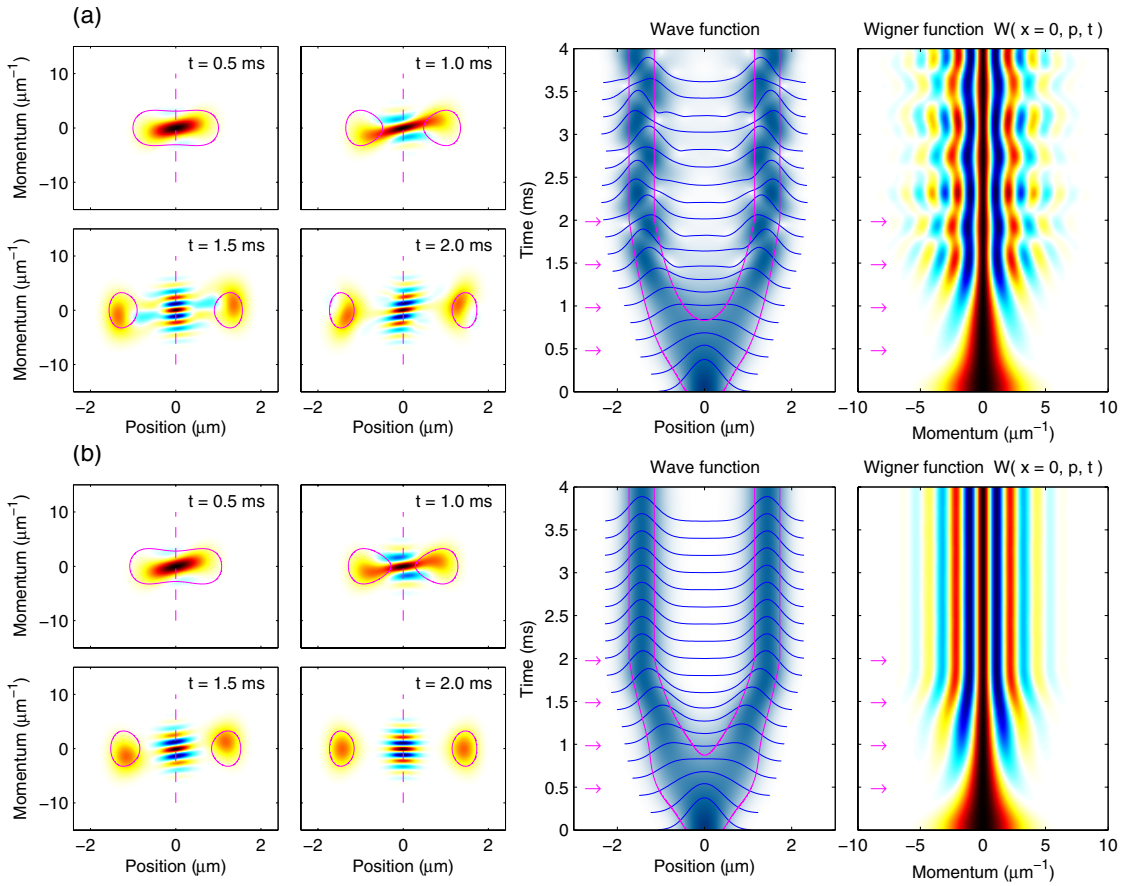

Fig. 2 (online colour at: www.fp-journal.org) Condensate splitting for (a) a control field $\lambda \propto \sqrt{t}$ and (b) the optimized control field. In both cases the splitting occurs for times below 2 ms, and λ is kept constant at later times. We use $U_0(N-1) = 1$. The different panels show snap shots of the Wigner function (left), a density plot of the wavefunction evolution $|\psi(x,t)|$ (middle), and the momentum distribution $w(0,p,t)$. In the middle panel we also depict the wavefunction modulus for selected times, and the contour line for $V_\lambda(x) = \mu_0$ where μ_0 is the mean particle energy in the initial condensate. Note that the interwell distance is directly related to the control parameter λ, and the equipotential lines thus provide direct information about $\lambda(t)$.

positive positions and momenta corresponds to that fraction of the condensate localized in the right well and moving to the right. At later times the left and right parts of the distribution still have finite momenta, thus indicating the condensate oscillations in the split trap. In addition, the Wigner function directly displays the interference properties of the split condensate, through the interference fringes around $x = 0$, which build up and sharpen when the left and right part of the condensate become separated.

A typical atom interferometer experiment consists of the condensate splitting, which is followed by a waiting phase, where one part of the condensate may acquire an additional phase due to the interaction with some external potential, and finally the condensate is released from the trap. Within the release process, the left and right part of the condensate start to overlap, and the interference in momentum space is transformed to an interference in position space, which can be directly monitored. An estimate for the fringe visibility is thus provided by the momentum distribution $w(0, p, t)$ of the Wigner function, whose time evolution is depicted in the right panel of Fig. 2. Due to the remaining oscillations in the split condensate, the interference fringes wiggle around and spoil the interferometer sensitivity.

It was shown in [19] that optimized time sequences for $\lambda(t)$, obtained within the framework of *optimal control theory* (OCT) [24], allow to completely suppress such oscillations. Some details of our approach are given in appendix A. Fig. 2(b) shows results of OCT simulations: one clearly observes that the small variations of $\lambda_{\rm opt}(t)$, with respect to the initial field, suffice to bring the condensate at the terminal time $T = 2$ ms to a complete halt. In [19] it was demonstrated that similar condensate trapping can be achieved for a variety of confinement potentials, and for a wide range of condensate nonlinearities and splitting times T.

3.2 Two-mode description

Let us investigate next condensate splitting within the framework of the two-mode model. When tunneling dominates over the nonlinearity, in the approximate groundstate all atoms reside in the bonding orbital $\psi_L + \psi_R$, which is the single-particle state of lowest energy. The resulting atom number distribution is a binomial one, since each atom has a fifty percent probability for localization in one of the wells. A convenient representation of the atom number distribution is on the Bloch sphere [23], Fig. 3: a state on the north pole would correspond to all atoms residing in the left well, and a state on the south pole to all atoms in the right well. All atoms in the bonding orbital corresponds to a state localized around $x = 1$, Fig. 3(a), whose width $1/\sqrt{N}$ is given by the fluctuations of the Gaussian state. On the other hand, for strong nonlinearities, i.e., $N\kappa \gg \Omega$, we can ignore the first part of the two-mode Hamiltonian (6), and obtain a Hamiltonian $\langle m|\hat{H}|m'\rangle \approx 2\kappa m^2\,\delta_{mm'}$ that is diagonal in the atom number imbalance m. In the state of lowest energy, half of the atoms sit in the left well and the other half in the right one. For finite tunneling, $\Omega < \kappa$, the state of lowest energy becomes a *squeezed state*, as depicted in Fig. 3(b), with finite atom number fluctuations below the value of the Gaussian state.

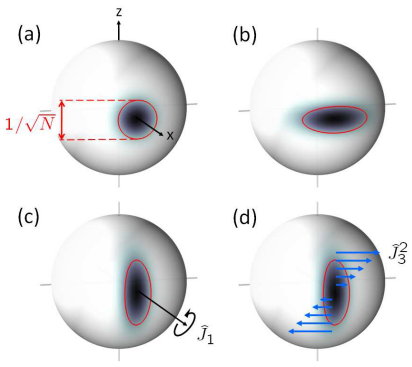

Fig. 3 (online colour at: www.fp-journal.org) Bloch-sphere representation of the atom-number distribution C: (a) Gaussian state with binomial atom number distribution, (b) number-squeezed, and (c,d) phase-squeezed state. (c) The action of the tunneling part of the Hamiltonian (6) corresponds to a rotation around the x-axis, and (d) the action of the nonlinear coupling to a polar-angle dependent rotation around the z-axis.

Squeezed states could help to significantly improve the performance of atom interferometers. To understand why, we first note that an interaction of the atoms in one of the wells with an external potential corresponds to a rotation of the atom-number state around the z-axis. This acquired phase is then read out either in a Michelson setup, by releasing the condensates and measuring the fringe positions, or in a Mach-Zehnder setup, by applying a $\pi/2$-tunneling pulse and transforming the phase information to an atom number difference, which can be directly measured [25]. Quite generally, *phase-squeezed states*, as shown in Fig. 3(c), would be the best for atom interferometry, as they would allow to perform measurements below the shot-noise limit of Gaussian states, ideally close to the Heisenberg limit. Unfortunately, the atom-atom interaction (which in typical ^{87}Rb atom chips experiments can not be manipulated through Feshbach resonances) would "wind up" a phase-squeezed state during the interferometer measuring time, as schematically indicated in Fig. 3(d). This would lead to phase diffusion that completely spoils the interferometer performance (see also discussion below). To minimize phase diffusion, it is beneficial to use *number-squeezed states*, Fig. 3(b), where the twist due to the nonlinear interaction has a much weaker effect.

Fig. 4 shows results of simulations for condensate splitting. We start in a state where tunneling dominates over the nonlinear coupling, and then exponentially turn off the tunnel coupling. If the turning-off is sufficiently slow, the system follows adiabatically in the state of lowest energy and finally ends up in a state with no atom number fluctuations. When the tunnel coupling is turned off faster, the system can follow adiabatically only up to a certain point and finally becomes frozen in a state with finite atom number fluctuations. As can be seen from the gray lines in Fig. 4, by increasing the decay constant of Ω by a factor of ten, the number fluctuations in the final state drop by a factor of approximately two. Thus, efficient atom number squeezing comes at the price of very slow splitting.

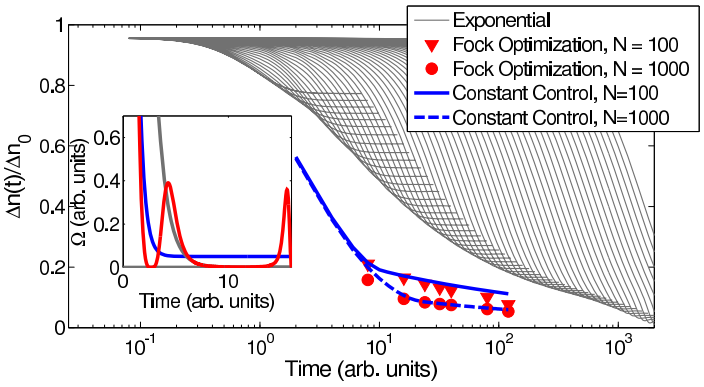

Fig. 4 (online colour at: www.fp-journal.org) Time evolution of the atom number fluctuations, in units of the fluctuations in the Gaussian state Δn_0, and for different atom numbers. The different curves correspond to an exponential turning-off of the tunneling, an OCT Fock optimization, and the two-parameter optimization described in the text. The inset reports typical time sequences for the tunnel coupling.

Optimization of number squeezing was recently presented in [26], where we found a control strategy that was interpreted in terms of a parametric oscillator model. With the H^1 norm discussed in appendix A, we now obtain more smooth control fields, shown in Fig. 4, which we denote as a *Fock optimization* (to be contrasted with the *Josephson optimization* of the parametric oscillator). The symbols in Fig. 4 show that over a wide range of times T, the optimized control fields perform significantly better than the exponential turning-off.

In the inset of the figure we show a typical OCT control field. After an initial stage of an exponential turning-off, the control has two main peaks. This control strategy can be understood in a Bloch-sphere representation as follows: in the first stage, the initial Gaussian state becomes twisted due to the nonlinear

interaction, see Fig. 3(d). The first control peak then rotates the twisted distribution around the x-axis, Fig. 3(c), where it ends up as a slightly rotated number-squeezed states. In between the two peaks the state then becomes further squeezed, due to the nonlinear interaction, and is further rotated by the second peak to its final position.

This control strategy is similar to that of Law et al. [27], who reported a scheme that exploits the combined effect of constant tunneling (rotation around x-axis) and nonlinear interaction (twist around z-axis). Indeed, if we keep the tunneling Ω after the first exponential turning-off constant, in the ensuing time evolution the distribution becomes twisted, due to the nonlinearity, and this twisted distribution is continuously rotated by the tunneling in such a manner that it ends up as a number-squeezed state. In Fig. 4 we show results for such a constant-control strategy, where we have optimized the turn-off time of the exponential decay as well as the value of the ensuing constant Ω-value. As can be seen, this more simple control performs equally well in comparison to the Fock optimization.

3.3 MCTDHB description

Finally, in Fig. 5 we show results for a full MCTDHB simulation of the splitting process. In Fig. 5(a), the time sequence of the control parameter $\lambda(t)$ has been chosen such that the decrease of the resulting tunnel coupling is approximately mono-exponential, in accordance to the two-mode model. One observes that during splitting an interference pattern builds up in the Wigner function. As time goes on, this pattern diminishes and finally almost disappears. This is due to the finite atom number fluctuations and the resulting phase diffusion, which strongly limits the performance of an atom interferometer.

In Fig. 5(b) we show results for an optimization of the full MCTDHB equations. Here, we have to fulfill the two control objectives of high number squeezing and final trapping of the condensate. As can be seen, OCT again comes up with a simple $\lambda(t)$ sequence, similar to the Fock optimization within the two-mode model, that leads to number squeezing values comparable to those of the two-mode model. This demonstrates that the simple two-mode model encapsulates all essential features of the number dynamics. As can be seen in the right panel of Fig. 5(b), number squeezing leads to a significantly extended visibility of the interference fringes, in comparison to the scheme depicted in panel (a).

Achieving a measurement sensitivity below the standard quantum limit requires reduced quantum fluctuations in the observable which is measured. Thus, in time-of-flight measurements the number squeezing must be transformed to phase squeezing, using $\pi/2$ tunnel pulses [28]. Alternatively, one can also transform the phase into number information [25]. However, these techniques are strongly limited by interactions. In both cases the phase sensitivity is given by the factor of "useful squeezing" [29] $\xi_R = 2\Delta n/\sqrt{N}\alpha$, which is small only for both small number fluctuations and good phase coherence $\alpha = 2\langle \hat{J}_x\rangle/N$. Below the shot noise limit we have $\xi_R < 1$, where ξ_R is bounded from below by the Heisenberg limit $\sqrt{2/N}$ [30]. In Fig. 6 it is shown that a good phase sensitivity, close to the Heisenberg limit, can be achieved much faster than with quasi-adiabatic exponential splitting. As our simulations are based on realistic microtrap potentials and include all pertinent physical mechanisms of the condensate dynamics, including both spatial and atom number degrees of freedom, we expect that our proposed schemes can be directly implemented in state-of-the-art atom chip experiments.

4 Summary and conclusions

We showed that applying optimal control techniques to the splitting of trapped atom clouds will allow to achieve high number squeezing much faster than with quasi-adiabatic splitting. This results in a significant enhancement of the coherence in trapped atom interferometers, and could help to significantly improve their performance. Nevertheless, even with squeezing during the splitting process the interaction-induced phase diffusion limits the measurement time in trapped atom interferometers.

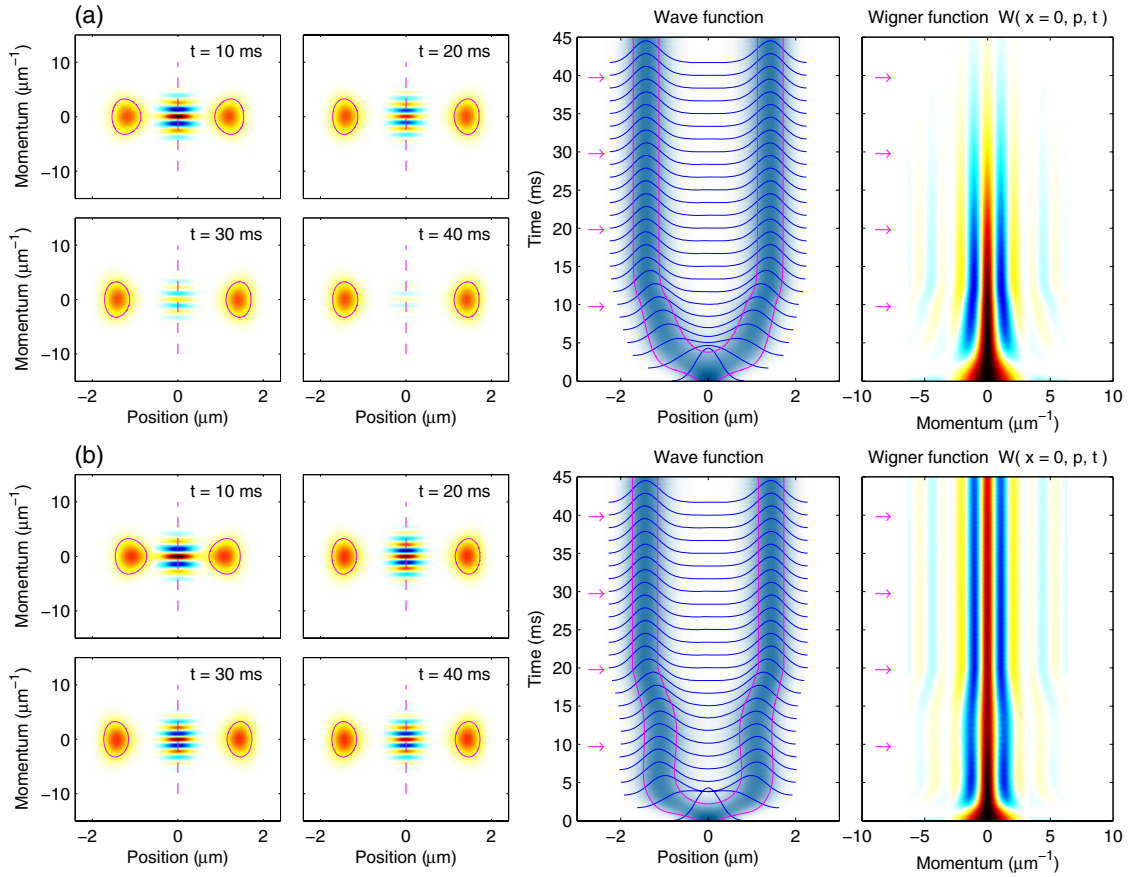

Fig. 5 (online colour at: www.fp-journal.org) Same as Fig. 2, but for the MCTDHB simulation, and for an (a) exponential turning-off of the tunnel control, and (b) a Fock optimization of $\lambda(t)$. The density matrix of the MCTDHB state is given by $\rho(x,x') = n_L\psi_L(x,t)\psi_L^*(x',t) + n_R\psi_R(x,t)\psi_R^*(x',t)$, where n_L and n_R are the populations of the left and right orbital, respectively. The Wigner function is obtained by taking the Fourier transform of $\rho(X+s/2, X-s/2)$ with respect to s.

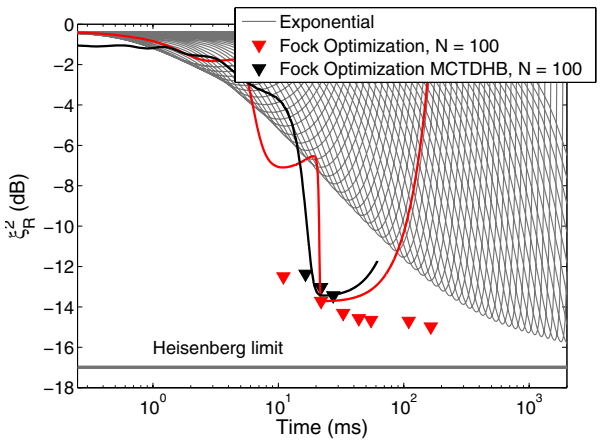

Fig. 6 (online colour at: www.fp-journal.org) Useful squeezing ξ for $N = 100$ and $U_0N = 1$, and for exponential (gray lines) and optimized (red triangles) turning-off of the tunnel control, as computed within the two-mode model. The black triangles report the results of MCTDHB simulations. The solid lines show selected examples for two-mode and MCTDHB simulations. For the exponential control, ξ drops to a certain value and then increases with increasing waiting time. In the optimized case, ξ drops to a much smaller value at a shorter time, where it remains constant for a period determined by the final value of the number fluctuations Δn.

Acknowledgements We thank Alfio Borzì, Greg von Winckel, Ofir Alon, and Thorsten Schumm for most helpful discussions. This work has been supported in part by the Austrian Science Fund FWF under project P18136–N13.

A Controlling the splitting and the interferometer performance

Can we do better than with control fields $\lambda(t)$ and $\Omega(t)$ chosen on the basis of physical intuition? In case of the Gross-Pitaevskii equation, can we bring the condensate to halt at short times? And for the two-mode model and MCTDHB, can we achieve higher number squeezing at short times? Both questions can be re-formulated within the framework of an optimization problem: we are seeking for the minimization of a quantity, the so-called *cost function*, subject to the constraint that the system is brought from an initial to a final state via a Schrödinger-type equation of motion. If we want to bring the orbitals to rest at the final time T, we can use a cost function of the form [19]

$$J(\psi,\lambda) = \frac{1}{2}\left(1 - \left|\langle\psi_d|\psi(T)\rangle\right|^2\right) + \frac{\gamma}{2}\int_0^T \left(\dot\lambda(t)\right)^2 dt\,. \tag{11}$$

Here ψ_d is the final, "desired" wavefunction, which corresponds to the groundstate of the split double well potential. The first part of the cost function is minimal when the final orbital $\psi(x,T)$ coincides with $\psi_d(x)$, modulo an arbitrary global phase. The second term on the rhs favors smooth control fields $\lambda(t)$ and is needed to make the optimal control problem well posed, as discussed below. γ is a weighting factor that determines the importance of the two control strategies of wavefunction matching and smooth control fields. We usually set $\gamma = 10^{-3}$ such that the first term in Eq. (11) is dominant. In case of number squeezing, we use a cost function of the form

$$J(C,\lambda) = \left(\left\langle \hat J_z^2\right\rangle - \left\langle \hat J_z\right\rangle^2\right) + \frac{\gamma}{2}\int_0^T \left(\dot\lambda(t)\right)^2 dt\,, \tag{12}$$

which becomes minimal for strongly number-squeezed states. In case of the two-mode model, the control parameter is the tunneling coupling $\Omega(t)$ rather than $\lambda(t)$, and the integrand in Eq. (12) should read $[\dot\Omega(t)]^2$.

Optimal control theory (OCT) aims at a minimization of the cost function, subject to the condition that the system evolves according to the dynamic equations discussed in Sects. 2.2—2.4. This can be done by employing Lagrange multipliers for the constraints and utilizing the fact that the Lagrange function has a saddle point at the minimum of J. For details, the interested reader is referred to the literature [19, 31]. Quite generally, one obtains three types of equations. First, the primary dynamic equations, which are initial value problems determined by the initial state associated with the single-well potential. Second, the sensitivity equations for the Lagrange multipliers, p, which describe how fluctuations evolve in a slightly perturbed system. In case of the Gross-Pitaevskii approach, we recover the Bogoliubov-de Gennes equations. Because the cost functions of Eqs. (11) and (12) only depend on the system properties at the final time T, the sensitivity equation forms a *terminal value problem* that has to be solved backwards in time, for the boundary value $p(T)$. Finally, we obtain an equation for the *optimal* control field $\lambda_{\rm opt}(t)$ in terms of the system variables and the Lagrange multipliers. All equations have to be fulfilled simultaneously for the optimal control.

In our numerical approach, we usually start with some initial guess for the control $\lambda(t)$ and solve the system equations forwards in time. Once the terminal value of the system variables is known, we can compute the terminal value for $p(T)$ and solve the sensitivity equation backwards in time. The two solutions ψ and p then allow us to obtain a search direction for an improved control, i.e., a λ-sequence that brings $\psi(T)$ closer to the desired solution. This equation reads, in case of the Gross-Pitaevskii equation [19],

$$\nabla J = -\gamma\frac{d^2\lambda}{dt^2} - \mathrm{Re}\,\langle\psi|\,\frac{\partial V_\lambda}{\partial\lambda}\,|p\rangle\ . \tag{13}$$

Similar expressions can be found for the two-mode model and MCTDHB. Once we have determined the search direction, we can obtain improved control fields by means of some minimization method, such as the nonlinear conjugate gradient approach or a quasi-Newton scheme. Details of this approach are described in [19, 26].

In some cases, there is a problem related to the numerical implementation of Eq. (13). It is a boundary value problem, where the endpoint conditions $\lambda(0) = 0$ and $\lambda(T) = 1$ imply that during the optimization process the potential is deformed from a single to a double well. For the initial guess one often ends up in a state that is quite far away from the desired solution. In turn, the terminal value for $p(T)$ is large and so is the gradient ∇J of Eq. (13). This has the consequence that the largest variation of the control field is initially at the terminal time T, while from a control perspective it would often be better to change the control at early times first. Only with increasing number of iterations in the minimization procedure the control becomes modified within the whole time interval. This can lead to a tedious and time-consuming optimization process.

A more convenient approach was recently formulated [32]. The main idea is to use a different norm in the integrals for the cost, Eqs. (11) and (12), as well as in the Lagrange function. For instance, in the cost functions the penalization for the control field $(\gamma/2)\left(\dot{\lambda},\dot{\lambda}\right)_{L^2}$ can be reformulated as $(\gamma/2)\left(\lambda,\lambda\right)_{H^1}$, where the definition of the H^1 inner product is $(u,v)_{H^1} = (\dot{u},\dot{v})_{L^2}$. It is important to realize that this different norm does neither affect the value of the cost function nor the principal or sensitivity equations. However, it does affect the equation for the control field, which now satisfies a Poisson equation

$$-\frac{d^2\,\nabla J}{dt^2} = -\gamma\frac{d^2\lambda}{dt^2} - \mathrm{Re}\,\langle\psi|\,\frac{\partial V_\lambda}{\partial\lambda}\,|p\rangle\ . \tag{14}$$

The advantage of Eq. (14) is that changes due to large values of the second term on the rhs are distributed, through the solution of the Poisson equation, over the whole time interval. In fact, most of our optimizations showed that the H^1 optimization is faster and more robust than the L^2 optimization, the resulting control fields are significantly smoother, and the global structure of $\lambda(t)$ is optimized. In this work we report throughout results for such H^1 optimizations.

References

[1] A. Cronin, J. Schmiedmayer, and D. Pritchard, Rev. Mod. Phys. **81**, 1051 (2009).

[2] S. Hofferberth, I. Lesanovsky, B. Fischer, T. Schumm, and J. Schmiedmayer, Nature **449**, 324–327 (2007).

[3] S. Hofferberth, I. Lesanovsky, T. Schumm, A. Imambekov, V. Gritsev, E. Demler, and J. Schmiedmayer, Nat. Phys. **4**, 489–495 (2008).

[4] R. Folman, P. Krüger, D. Cassettari, B. Hessmo, T. Maier, and J. Schmiedmayer, Phys. Rev. Lett. **84**, 4749 (2000).

[5] R. Folman, P. Krüger, J. Schmiedmayer, J. Denschlag, and C. Henkel, Adv. in Atom. Mol. and Opt. Phys. **48**, 263 (2002).

[6] J. Fortagh and C. Zimmermann, Rev. Mod. Phys. **79**, 235 (2007).

[7] T. Schumm, S. Hofferberth, L. M. Andersson, S. Wildermuth, S. Groth, I. Bar-Joseph, J. Schmiedmayer, and P. Krüger, Nat. Phys. **1**, 57–62 (2005).

[8] Y. J. Wang, D. Z. Anderson, V. M. Bright, E. A. Cornell, Q. D., T. Kishimoto, M. Prentiss, R. A. Saravanan, S. R. Segal, and S. Wu, Phys. Rev. Lett. **94**(7), 090405 (2005).

[9] M. Albiez, R. Gati, J. Fölling, S. Hunsmann, M. Cristiani, and M. K. Oberthaler, Phys. Rev. Lett. **95**, 010402 (2005).

[10] D. Cassettari, A. Chenet, R. Folman, A. Haase, B. Hessmo, P. Krüger, T. Maier, S. Schneider, T. Calarco, and J. Schmiedmayer, Appl. Phys. B **70**, 721 (2000).

[11] W. Hänsel, J. Reichel, P. Hommelhoff, and T. W. Hänsch, Phys. Rev. A **64**, 063607 (2001).

[12] I. Lesanovsky, T. Schumm, S. Hofferberth, L. M. Andersson, P. Krüger, and J. Schmiedmayer, Phys. Rev. A **73**(3), 033619 (2006).

[13] J. Javanainen and M. Y. Ivanov, Phys. Rev. A **60**, 2351 (1999).

[14] C. Henkel, P. Krüger, R. Folman, and J. Schmiedmayer, Appl. Phys. B **76**, 173 (2003).
[15] G. B. Jo, Y. Shin, S. Will, T. A. Pasquini, M. Saba, W. Ketterle, D. E. Pritchard, M. Vengalattore, and M. Prentiss, Phys. Rev. Lett. **98**, 030407 (2007).
[16] J. Esteve, C. Gross, A. Weller, S. Giovanazzi, and M. K. Oberthaler, Nature **455**, 1216 (2008).
[17] F. Dalfovo, S. Giorgini, L. P. Pitaevskii, and S. Stringari, Rev. Mod. Phys. **71**, 463 (1999).
[18] A. Leggett, Rev. Mod. Phys. **73**, 307 (2001).
[19] U. Hohenester, P. K. Rekdal, A. Borzi, and J. Schmiedmayer, Phys. Rev. A **75**, 023602 (2007).
[20] J. Grond, G. von Winckel, J. Schmiedmayer, and U. Hohenester, arXiv:0908.1634, to appear in Rev. Phys. A.
[21] G. J. Milburn, J. Corney, E. M. Wright, and D. F. Walls, Phys. Rev. A **55**, 4318 (1997).
[22] O. E. Alon, A. I. Streltsov, and L. S. Cederbaum, Phys. Rev. A **77**, 033613 (2008).
[23] F. T. Arecchi, E. Courtens, R. Gilmore, and H. Thomas, Phys. Rev. A **6**, 2211 (1972).
[24] A. P. Peirce, M. A. Dahleh, and H. Rabitz, Phys. Rev. A **37**, 4950 (1988).
[25] L. Pezzé, L. A. Collins, A. Smerzi, G. P. Berman, and A. R. Bishop, Phys. Rev. A **72**, 043612 (2005).
[26] J. Grond, J. Schmiedmayer, and U. Hohenester, Phys. Rev. A **79**, 021603(R) (2009).
[27] C. K. Law, H. T. Ng, and P. T. Leung, Phys. Rev. A **63**, 055601 (2001).
[28] M. Jääskeläinen, W. Zhang, and P. Meystre, Phys. Rev. A **70**(6), 063612 (2004).
[29] D. J. Wineland, J. J. Bollinger, W. M. Itano, and D. J. Heinzen, Phys. Rev. A **50**, 67 (1994).
[30] V. Giovannetti, S. Lloyd, and L. Maccone, Science **306**, 1330 (2004).
[31] A. Borzì, G. Stadler, and U. Hohenester, Phys. Rev. A **66**, 053811 (2002).
[32] G. von Winckel and A. Borzi, Inverse Problems **24**, 034007 (2008).

